ARMY RESEARCH LABORATORY

Signal Modeling of Turbulence-Distorted Imagery

by S. Susan Young, Ron Driggers, Keith Krapels, Richard Espinola, Joseph Reynolds, and Jae Cha.

ARL-RP-0275 **September 2009**

A reprint from *Proc. SPIE*, vol. 7300 73000P (2009) from the *SPIE Defense, Security, and Sensing (Dss09)*, Orlando, FL, April 13–17, 2009.

NOTICES

Disclaimers

The findings in this report are not to be construed as an official Department of the Army position unless so designated by other authorized documents.

Citation of manufacturer's or trade names does not constitute an official endorsement or approval of the use thereof.

Destroy this report when it is no longer needed. Do not return it to the originator.

Army Research Laboratory
Adelphi, MD 20783-1197

ARL-RP-0275 **September 2009**

Signal Modeling of Turbulence-Distorted Imagery

S. Susan Young
Sensors and Electron Devices Directorate, ARL

Ronald Driggers
Naval Research Laboratory, Washington DC

Keith Krapels, Richard L. Espinola, Joseph R. Reynolds, and Jae Cha
Night Vision & Electonic Sensors Directorate, FT Belvoir, VA

A reprint from *Proc. SPIE*, vol. 7300 73000P (2009) from the *SPIE Defense, Security, and Sensing (Dss09)*, Orlando, FL, April 13–17, 2009.

REPORT DOCUMENTATION PAGE	Form Approved OMB No. 0704-0188

1. REPORT DATE *(DD-MM-YYYY)*	2. REPORT TYPE	3. DATES COVERED (From - To)
September 2009	Summary	

4. TITLE AND SUBTITLE	5a. CONTRACT NUMBER
Signal Modeling of Turbulence-distorted Imagery	5b. GRANT NUMBER
	5c. PROGRAM ELEMENT NUMBER

6. AUTHOR(S)	5d. PROJECT NUMBER
S. Susan Young, Ronald G. Driggers, Keith Krapels, Richard L. Espinola, Joseph P. Reynolds, and Jae Cha	5e. TASK NUMBER
	5f. WORK UNIT NUMBER

7. PERFORMING ORGANIZATION NAME(S) AND ADDRESS(ES)	8. PERFORMING ORGANIZATION REPORT NUMBER
U.S. Army Research Laboratory ATTN: RDRL-SES-E 2800 Powder Mill Road Adelphi, MD 20783-1197	ARL-RP-0275

9. SPONSORING/MONITORING AGENCY NAME(S) AND ADDRESS(ES)	10. SPONSOR/MONITOR'S ACRONYM(S)
	11. SPONSOR/MONITOR'S REPORT NUMBER(S)

12. DISTRIBUTION/AVAILABILITY STATEMENT

Approved for public release; distribution unlimited.

13. SUPPLEMENTARY NOTES

A reprint from *Proc. SPIE*, vol. 7300 73000P (2009) from the *SPIE Defense, Security, and Sensing (Dss09)*, Orlando, FL, April 13–17, 2009.

14. ABSTRACT

Understanding turbulence effects on wave propagation and imaging systems has been an active research area for more than 50 years. Conventional atmospheric optics methods use statistical models to analyze image degradation effects that are caused by turbulence. In this paper, we intend to understand atmospheric turbulence effects using a deterministic signal processing and imaging theory point of view and modeling. The model simulates the formed imagery by a lens by tracing the optical rays from the target through a band of turbulence. We examine the nature of the turbulence-degraded image, and identify its characteristics as the parameters of the band of turbulence, e.g., its width, angle, and index of refraction, are varied. Image degradation effects due to turbulence, such as image blurring and image dancing, are revealed by this signal modeling. We show that in fact these phenomena can be related not only to phase errors in the frequency domain of the image but also a 2D modulation effect in the image spectrum. Results with simulated and realistic data are provided.

15. SUBJECT TERMS

Atmospheric turbulence effects, turbulence-distorted imagery, signal modeling

16. SECURITY CLASSIFICATION OF:			17. LIMITATION OF ABSTRACT	18. NUMBER OF PAGES	19a. NAME OF RESPONSIBLE PERSON
a. REPORT	b. ABSTRACT	c. THIS PAGE			S. Susan Young
Unclassified	Unclassified	Unclassified	UU	18	19b. TELEPHONE NUMBER (*Include area code*) (301) 394-0230

Standard Form 298 (Rev. 8/98)
Prescribed by ANSI Std. Z39.18

Signal Modeling of Turbulence-Distorted Imagery

S. Susan Young[a], Ronald G. Driggers[b], Keith Krapels[c]
Richard L. Espinola[c], Joseph P. Reynolds[c], and Jae Cha[c]
[a]Army Research Laboratory, 2800 Powder Mill Rd, Adelphi, MD 20783
[b]Naval Research Laboratory, 4555 Overlook Ave, Washington DC 20375
[c]Night Vision & Electronic Sensors Directorate, 10221 Burbeck Rd, Fort Belvoir, VA 22060
Email: ssyoung@arl.army.mil

ABSTRACT

Understanding turbulence effects on wave propagation and imaging systems has been an active research area for more than 50 years. Conventional atmospheric optics methods use statistical models to analyze image degradation effects that are caused by turbulence. In this paper, we intend to understand atmospheric turbulence effects using a deterministic signal processing and imaging theory point of view and modeling. The model simulates the formed imagery by a lens by tracing the optical rays from the target through a band of turbulence. We examine the nature of the turbulence-degraded image, and identify its characteristics as the parameters of the band of turbulence, e.g., its width, angle, and index of refraction, are varied. Image degradation effects due to turbulence, such as image blurring and image dancing, are revealed by this signal modeling. We show that in fact these phenomena can be related not only to phase errors in the frequency domain of the image but also a 2D modulation effect in the image spectrum. Results with simulated and realistic data are provided.

Keywords: atmospheric turbulence effects, turbulence-distorted imagery, signal modeling, Fourier analysis, imaging theory.

1. INTRODUCTION

Atmosphere turbulence is one of many factors that affect sensor performance and image quality. It results in distorted imagery such as “image blur” and “image dancing” degradations. In order to design an effective signal processing technique to remove the turbulence degradation phenomenon or improve the image quality, it is important to understand the turbulence effects and sources of degradation first from a signal processing and imaging theory point of view.

Understanding turbulence effects on wave propagation and imaging systems has been an active research area for more than 50 years. Conventional atmospheric optics methods use statistical models to analyze image degradation effects that are caused by turbulence [1-2]. These methods have followed the theoretical basis from contributions of Kolmogorov [3] for developing a statistical model for the spatial structure of turbulent air flows, Tatarskii [4] for applying Kolmogorov’s model to the problems of wave equation and propagation through regions of weak random index fluctuation, and Fried [5] for extending Tatarskii’s results to describe turbulence effects on the resolution of imaging systems.

Image degradation effects due to turbulence include image blur and image dancing [1]. Conventionally, many research showed that turbulence-induced wave propagation variations across the aperture of an imaging system distort the point spread function (PSF) of the imaging system. The influence of turbulence blur to image blur effects has been characterized in terms of a modulation transfer function (MTF) from the atmosphere, that was derived by Goodman [6], Hufnagel et al, [7] and Fried [8]. Later work on the model for turbulence MTF was extended on the imaging systems in the visible and infrared bands [9-10]. The evaluations and validations of the turbulence MTF in the infrared imagery were conducted in Ref. 11-12. However, it has also shown [1,13] that wave propagation through turbulence results in a phase error in the frequency domain of the recorded image. One of our objectives in this paper is to characterize the image blur effect in terms of a spectral domain phase degradation.

Various statistical descriptions of the optical wave through random media are also used to characterize the image degradation effects. For example, the angle-of-arrival fluctuations of an optical wave in the plane of the receiver aperture are associated with image dancing in the focal plane of an imaging system [1]. The beam wander was also characterized statistically by the variance of the beam displacement along an axis or by the variance of the magnitude of the beam displacement. This phenomenon is also related to image dancing.

The phase screen method is another extending development to model the propagation of an optical wave as a limiting case of extended turbulence confined to a thin slab screen between the transmitter and receiver [14]. There are a number of approaches to generate random phase screens with the proper point statistics and spatial and temporal correlation properties [1-2, 14-15]. The thin phase screen models permit the experimentalist to predict statistical results associated with laboratory experiments. However, it requires critical placement of the phase screen with respect to transmitter and receiver [1].

Intuitively, the image dancing degradation is caused by the temporal variations of the turbulence-distorted imagery. Unlike conventional statistical models, another objective in this paper is to characterize the image dancing effect using a Fourier spectral analysis of recorded images.

In this paper, we intend to understand atmospheric turbulence effects using deterministic signal modeling and imaging theory. Our model simulates the formed imagery by a lens by tracing the optical rays from the target through a band of turbulence. We examine the nature of the turbulence-degraded image, and identify its characteristics as the parameters of the band of turbulence, e.g., its width, angle, and index of refraction, are varied. Image degradation effects due to turbulence, such as image blur and image dancing, are revealed by this signal modeling. We show that in fact these phenomena can be related not only to phase errors in the frequency domain of the image but also a 2D modulation effect in the image spectrum.

The paper is organized as follows. The signal propagation model and imaging without and with turbulence, for parallel and slanted turbulence, are presented in Section 2. This signal modeling is used to characterize the image blur due to turbulence in terms of the magnitude and phase degradations that are presented in Section 3. Section 4 presents a method to examine the spectral properties of the turbulence-distorted images that are related to image dancing phenomenon. The results of magnitude and phase degradations of simulated data are presented in Section 5. Spectral properties of real field data are presented in Section 6. The summary is provided in Section 7.

2. SIGNAL MODELING

2.1 Signal Propagation Model and Imaging

Fig. 1 illustrates the geometry of image formation [16] using the signal propagation modeling. Assume the target is a planar target with an area of $(-Y_0, Y_0)$. Each point of the target emits a time-dependent signal with a known frequency ω or wavelength λ [$\omega = (2\pi c)/\lambda$], c is the speed of the light, that is, $p(t) = \exp(j\omega t)$. We examine the signal that is emitted by the target and is received at the lens with a size of $u \in (-L, L)$. The image formed by the lens is calculated using a wavefront reconstruction method [17]. As a result, the image distortion is due to the turbulence only since the wavefront reconstruction is approximation free.

The x-coordinate is used to identify range from the target to the lens, and y specifies the cross-range domain. The lens is located on the line $x = X_c$ and identified by (X_c, u). The time delay of the signal propagation from (x, y) in the target region to an aperture point on the lens is

$$\tau_0 = \frac{\sqrt{X_c^2 + (u-y)^2}}{c} = \frac{d(u)}{c} \tag{1}$$

where $d(u) = \sqrt{X_c^2 + (u-y)^2}$ is the distance the signal travels from the target to the aperture point. The total signal received at the lens is obtained from the analysis of wavefront reconstruction imaging method in [17]:

$$s(u,t) = \int_y f(y,t)\exp[\,j\omega t + j\phi(y,t)]\exp[\,j\,k\,d(u)]\,dy \tag{2}$$

The function $f(y,t)$ is the reflectance map function (related to the desired image) that contains both the target's physical properties and fluctuations of the amplitude of radiating (emitting) source; and $\phi(y,t)$ is an unknown phase function that represents the relative phase delay of the imaging wave on a target point (related to the distance between the source and the point target and the unknown phase fluctuations of the source), and the lack of coherence among the target's radiating points and the receiver structure for the passive array. The variable k is the wavenumber, $k = \omega / c$. For simplicity, we define

$$g(y,t) = f(y,t)\exp[\,j\phi(y,t)]$$

Following the analysis in [17], after taking the spatial Fourier transform of both side of (2) with respect to u, we obtain

$$G_y(k_u,t) = \exp(-j\omega t)\exp[-j(\sqrt{k^2 - k_u^2}\,X_c)\,S(k_u,t) \tag{3}$$

where $G_y(k_u,t)$ is the Fourier transform of the image formed, $S(k_u,t)$ is the Fourier transform of the measured signal at the lens, and k_u is the frequency of the aperture element u. The reconstructed signal $g(y,t)$ is simply the inverse transform of $G_y(k_u,t)$.

For a narrow band or a single frequency source, the reconstructed signal $g(y,t)$ can be denoted as the function of $g(y)$ [15-16]. This is based on the fact that the recorded image is the integration of the measurements over a period of time, T, e.g., the camera integration time, i.e.,

$$g(y) = \int_T |g(y,t)|dt$$

For a wide band signal, e.g., a longwave infrared signal with a bandwidth of $8-12\,\mu$m (micrometers), the bandwidth is divided into a number of narrow wavelength bands. Then the signal is reconstructed for each wavelength band.

2.2 Imaging in Present of Turbulence

Now, we consider the imaging system geometry when a band of turbulence of width D is present in Figs. 2-3. The main factor that has to be incorporated in this scenario is the effect of turbulence in the time delay of propagated waves. We divide the distance that the signal travels from the target to the element into three portions, d_1, d_2, and d_3, as shown in Figs. 2-3. In this case, d_1 represents the wave propagation path from the target to the entry point of the turbulence, d_2 the path inside the turbulence, and d_3 the path from the exit point of the turbulence to the lens. The total time delay for the wave propagation is obtained as

$$\tau = \frac{d_1}{v_1} + \frac{d_2}{v_2} + \frac{d_3}{v_3}\ ,\quad v_1 = v_3 = c\ ,\quad v_2 = c/n_2 \tag{4}$$

where n_2 is the index of refraction of the material (substance) in the turbulence band.

The signal received at the lens can be rewritten as follows:

$$s(u,t) = \int_{-Y_0}^{Y_0} f(y,t)\exp[\,j\omega t + j\phi(y,t)]\exp[\,j\,(k_1 d_1 + k_2 d_2 + k_1 d_3)]\,dy \tag{5}$$

where $k_2 = k_1 / n$ and k_1 is the wavenumber of the air. After the distances of d_1, d_2, and d_3 are calculated, the reconstructed signal is obtained the same way as in (3).

In the following, we determine the distances of d_1, d_2, and d_3 using ray tracing. We consider two scenarios of turbulence: 1) parallel turbulence in which the turbulence is parallel with the target and sensor (see Fig. 2); 2) slanted turbulence in which the turbulence has a slanted angle with respect to the target and sensor (see Fig. 3).

2.2.1 Parallel Turbulence

Fig. 2 shows the signal propagation geometry when a band of turbulence is parallel with the target and sensor plane. The signal entrance angles in the air, turbulence band, and out the air are identified as θ_1, θ_2, and θ_1, respectively. According to the Snell law, we have

$$n_1 \sin\theta_1 = n_2 \sin\theta_2 \tag{6}$$

where n_1 and n_2 are the index of refraction of the air and the turbulence, respectively. From the geometry in Fig. 2, we have following:

$$y_t = y_1 + y_2 + y_3 \tag{7}$$

where the variables y_1, y_2, y_3, and y_t are the distances defined in Fig. 2. According to the signal propagation geometry shown in Appendix A, the value of $\sin\theta_1$ is solved by minimizing the following for a given point target at (x, y) and every element of the aperture (that is u):

$$\min_{\theta_1} (y_1 + y_2 + y_3 - y_t) \tag{8}$$

The distances of d_1, d_2, and d_3 can be obtained from the value of $\sin\theta_1$, the target range, turbulence width, and the distance from the turbulence to the lens as shown in Fig. 2.

2.2.2 Slanted Turbulence

Fig. 3 shows the signal propagation geometry when a band of turbulence has a slanted angle θ_r with respect to the target and sensor plane. Now, the equation of (7) is still satisfied in the slanted direction with angle θ_r as shown in Appendix B. Similarly, the value of $\sin\theta_1$ is solved by minimizing the following:

$$\min_{\theta_1} (y_1 + y_2 + y_3 - y_t) \tag{9}$$

3. MAGNITUDE AND PHASE DEGRADATIONS

Literatures [1, 13] show that turbulence causes a phase error in the frequency domain of the recorded image. Using the signal modeling described in the previous section allows us to study the nature of the turbulence-degraded images in terms of both magnitude and phase degradations. The magnitude degradation is a straight forward analysis by the above mentioned signal modeling and is demonstrated in Section 5. The analysis of the phase degradation due to turbulence is presented in this section.

Let $G(k_y)$ and $G_1(k_y)$ be Fourier transforms of $g(y)$ and $g_1(y)$, respectively. If there is a phase difference $\varphi(k_y)$ between two signals, $G(k_y)$ and $G_1(k_y)$, we have:

$$G(k_y) = G_1(k_y) \exp[j\, \varphi(k_y)] \tag{10}$$

The phase difference $\varphi(k_y)$ can be obtained from calculating the phase angle of the correlation function $F_c(k_y)$, that is obtained as follows:

$$F_c(k_y) = G(k_y)\, G_1^*(k_y) = \left|G_1(k_y)\right|^2 \exp[-j\varphi(k_y)] \tag{11}$$

The phase angle is a 1D function with respect to the frequency domain k_y.

4. SPECTRAL PROPERTIES

Image dancing is a degradation caused by the temporal variations of the turbulence-distorted imagery. In this section, we examine the spectral properties of the turbulence-distorted images. We contemplate that what is

referred to as “dancing” or “waving” in images that are degraded by turbulence is in fact a modulation phenomenon.

As it is known, the shift of the spectrum of the image causes the modulation in the spatial domain. The IR or visible camera is a non-coherent imaging system. Thus, the recorded image is a full-wave rectified version of the reconstruction. We anticipate to see the properties that are associated with the spectrum of a full-wave rectified signal.

To study the spectral properties of the image, we calculate the 3D spectrum. Consider an image sequence be $f(x,y,t)$ and denote its 3D Fourier transform by $F(k_x,k_y,\omega)$. The 1D power spectrum with respect to the time domain can be obtained by the following:

$$S_1(\omega)=\sum_{k_x}\sum_{k_y}\left|F(k_x,k_y,\omega)\right|^2 \tag{12}$$

Similarly, the power spectrum with respect to the x domain is obtained by the following:

$$S_2(k_x)=\sum_{k_y}\sum_{\omega}\left|F(k_x,k_y,\omega)\right|^2 \tag{13}$$

The power spectrum with respect to the y domain is obtained by the following:

$$S_3(k_y)=\sum_{k_x}\sum_{\omega}\left|F(k_x,k_y,\omega)\right|^2 \tag{14}$$

We also consider the 2D power spectrum with respect to the time domain by the following:

$$S_4(k_x,k_y)=\sum_{\omega}\left|F(k_x,k_y,\omega)\right|^2 \tag{15}$$

By studying the power spectrum in the time, x, and y domains separately, we can examine the spectral properties of image affected by turbulence. This helps us identify the problem analytically and understand the turbulence phenomena.

5. MAGNITUDE AND PHASE DEGRADATIONS OF SIMULATED DATA

In this section, we present the simulated imagery using the signal modeling method described in Sections 2-3. We examine the nature of the turbulence-degraded image and identify its characteristics as the parameters of the band of turbulence are varied.

There are three types of the parameters in the signal modeling to describe the lens, the target, and the band of turbulence, respectively. Referring to Figs. 2-3, the parameters can be divided into three groups in the following.

The parameters of lens include: the size of the lens, L. The parameters of the target include: the location of the target, (x,y); the area of the target, Y_0; and the wavelength of the target, λ. The parameters of the turbulence include: the index of refraction, n_2; the width of the turbulence, D; the slanted angle, θ_r; and the distance between the turbulence to lens, x_{r0}. Varying above parameters, we form the signals, $g(y)$ and $g_1(y)$, with and without turbulence, respectively.

5.1 Magnitude Degradation due to Turbulence

5.1.1 Varying Turbulence Index of Refraction

Fig. 4 shows the magnitudes of signals, $g(y)$ and $g_1(y)$, with and without turbulence, respectively, for the cases of the index of refraction being $n_2=1.5$ and 2.

The parameter of the lens is $L = 0.2$ m. The parameters of the target are $(x, y) = (X_c, 0)$, $X_c = 100$ m, $Y_0 = 0.5$ m, and $\lambda = 8 - 12\mu$m (longwave infrared). We divide the wavelengths into 4 narrow wavelength bands. Other parameters of the band of the turbulence are $D = 10$ m, $\theta_r = 0^0$, and $x_{r0} = 50$ m.

The solid lines in Fig. 4 represent the magnitude of signal with turbulence, $g(y)$, the dotted lines the signal without turbulence, $g_1(y)$, for the first wavelength band. From Fig. 4, comparing with $g_1(y)$, $g(y)$ becomes more smeared when the index of refraction n_2 increases. This indicates that larger index of refraction of the turbulence causes more degradation of the signal.

5.1.2 Varying Turbulence Width

Fig. 5 shows the magnitudes of signals, $g(y)$ and $g_1(y)$, with and without turbulence, respectively, for the cases of the width of the turbulence being $D = 10$ m and 20m.

The parameter of the lens is $L = 0.2$ m. The parameters of the target are $(x, y) = (X_c, 0)$, $X_c = 100$ m, $Y_0 = 0.5$ m, and $\lambda = 8 - 12\mu$m (longwave infrared). The wavelength is divided into 4 wavelength bands. Other parameters of the band of the turbulence are $n_2 = 2$, $\theta_r = 0^0$, and $x_{r0} = 50$ m.

The solid lines in Fig. 5 represent the magnitude of signal with turbulence, $g(y)$, the dotted lines the signal without turbulence, $g_1(y)$. From Fig. 5, comparing with $g_1(y)$, $g(y)$ becomes more smeared when the width of the turbulence D increases. This also indicates that the thicker layer of the turbulence causes more degradation of the signal.

5.1.3 Varying Turbulence Slanted Angle

Figs. 6-7 show the magnitudes of signals, $g(y)$ and $g_1(y)$, with and without turbulence, respectively, for the cases of the slanted angle of the turbulence being $\theta_r = 10^0$ and 20^0.

The parameter of the lens is $L = 0.2$ m. The parameters of the target are $(x, y) = (X_c, 0)$, $X_c = 100$ m, $Y_0 = 5$ m, and $\lambda = 8 - 12\mu$m (longwave infrared). The wavelength is divided into 4 wavelength bands. Other parameters of the band of the turbulence are $D = 10$ m, $n_2 = 2$, and $x_{r0} = 50$ m.

The solid lines in Figs. 6-7 represent the magnitude of signal with turbulence, $g(y)$, the dotted lines the signal without turbulence, $g_1(y)$, for the first wavelength band. From Fig. 6, the signal $g(y)$ has a shift from $g_1(y)$. When the slanted angle of the turbulence increases, this shift increases too. Fig. 7 shows the signals that are zoomed in around the central point. Comparing with $g_1(y)$, $g(y)$ appears smeared. This indicates that the turbulence not only causes the signal blurred, but also the signal shifted when the turbulence has a slanted angle.

If one is targeting an object when the turbulence presents, the location of the object that appears in the image could be shifted from the real location when the turbulence appears at a slanted angle. This needs to be corrected for turbulence-distorted imagery.

5.2 Phase Degradation due to Turbulence

In this section, we study the signal phase degradation due to the turbulence using the method presented in Section 3. The parameter of the lens is $L = 0.2$ m. The parameters of the target are $(x, y) = (X_c, 0)$, $X_c = 100$ m, $Y_0 = 0.5$ m,

and $\lambda = 8-12\mu$m (longwave infrared). The wavelength is divided into 4 wavelength bands. The fixed parameters of the band of the turbulence are $\theta_r = 0^0$ and $x_{r0} = 50$ m. We vary the turbulence width and index of refraction in the following 2 cases: 1) $D = 10$ m, $n_2 = 1.5$; 2) $D = 20$ m, $n_2 = 2$.

The solid lines in Fig. 8 show the phase angle curves, $\varphi(k_y)$, of the correlation function $F_c(k_y)$ in (11) for the above 2 cases using the first wavelength band. The central part of the phase angle curve appears to be a Gaussian function. We then fit the Gaussian function to the phase angle curve. The Gaussian function of the phase angle with respect to the frequency domain, k_y, is defined as:

$$\varphi(k_y) = A\exp(-\frac{k_y^2}{2\sigma^2}) = A\exp(-\alpha k_y^2)$$

where the parameter A determines the amplitude, $\alpha = 1/(2\sigma^2)$, which is inversely proportional to the standard deviation of the Gaussian function. The fitted Gaussian function curves are plotted as dotted lines in Fig. 8. The parameters (A,α) that are used to fit the Gaussian functions for the above 2 cases are also listed in Fig. 8.

This study shows that the phase angle due to the turbulence is a Gaussian function instead of a quadratic function. This indicates that the correction of the image blurring caused by the turbulence due to the phase degradation could be realized by searching the parameter space of (A,α).

6. SPECTRAL PROPERTIES OF REAL DATA

A sequence of 60 frames of a natural scene with turbulence is selected. Fig. 9(a) shows one of the frames from this sequence. The spectrum with respect to the time, x, and y domains are shown in Figs. 9(b)-(d), respectively. From Fig. 9(b), the spectrum shows weak harmonics. That indicates that a minor degree of waving appears in the time domain. The spectrum with respect to x domain that is shown in Fig. 9(c) does not show strong harmonics, which indicates the waving does not appear, or not easy to be observed, in the x domain, the vertical direction. This is indeed the case from viewing the video. Fig. 9(d) shows the spectrum with respect to y domain and it shows strong harmonics. This indicates the strong waving in the y domain, the horizontal direction. Indeed, the video of the sequence shows the strong waving appearance in the horizontal direction.

Figs. 9(e)-(f) show the 2D power spectral properties of this sequence. The 2D power spectrum with respect to the time domain is defined in (15). The distributions of the power spectrum at $k_y = 0$ and $k_x = 0$ are shown in Figs. 9(e) and (f), respectively. Fig. 9(e) does not illustrate prominent harmonics. Meanwhile, Fig. 9(f) shows strong harmonics. This corresponds to the fact that there is no obvious waving appearance in the vertical direction (x) but waving in the horizontal direction (y).

Next, a sequence of 100 frames of a test bar pattern scene with turbulence [18] is selected. Fig. 10(a) shows one of the frames from the sequence, which exhibits a strong turbulence; in this case, the test bar pattern is severely distorted. The spectrum with respect to the time, x, and y domains are shown in Figs. 10(b)-(d), respectively. Figs. 10(b)-(c) do not show prominent harmonics. The video of the sequence verifies that there is no obvious waving in the time domain and the vertical direction (x). However, strong harmonics can be seen around the middle frequency in Fig. 10(d). Indeed, the video shows a strong waving in the horizontal direction (y). There are also some fluctuations near the zero frequency in Fig. 10(d). This is the natural look of the spectrum of the test pattern.

Figs. 10(e)-(f) show the 2D power spectral distribution of this sequence. The distributions of the power spectrum at $k_y = 0$ and $k_x = 0$ are shown in Fig. 10(e) and (f), respectively. There are no prominent harmonics illustrated

in Fig. 10(e). Meanwhile, strong harmonics are shown in Fig. 10(f). These also correspond to the fact that there is no obvious waving in the vertical direction (x) but there is strong waving in the horizontal direction (y).

Last, a sequence of 100 frames of a test bar pattern scene with weak turbulence [18] is selected. Fig. 11(a) shows one of the frames of this sequence, which exhibits a weak turbulence. The video of the sequence shows no obvious waving in the time domain and the vertical direction (x), and weak waving in the horizontal direction (y). These are shown in the spectrum with respect to the time, x , and y domains in Figs. 11(b)-(d), respectively. That is, there are no obvious harmonics in Figs. 11(b)-(c) and possible weak harmonics in the lower frequency band in Fig. 11(d). In Fig. 11(d), harmonics are also present near the zero frequency of the spectrum. This is also the natural look of the spectrum of the test pattern that is approximately a periodic signal.

Figs. 11(e)-(f) shows the 2D power spectral distribution of this sequence. The distributions of the power spectrum at $k_y = 0$ and $k_x = 0$ are shown in Fig. 11(e) and (f), respectively. Fig. 11(e) does not present prominent harmonics. Fig. 11(f) shows weak harmonics. This also reflects the fact that there is no obvious waving in the vertical direction (x) but there is weak waving in the horizontal direction (y).

7. SUMMARY

In this paper, we presented a signal modeling method to study the nature of a turbulence-degraded image. The proposed signal modeling was used to identify a turbulence-distorted image's characteristics as the parameters of the band of turbulence, e.g., its width, angle, and index of refraction, are varied. The magnitude and phase degradations, and spectral properties of the simulated data and field trial imagery data with turbulence were demonstrated. These include image degradations due to turbulence, such as image blurring and image dancing phenomena. The results illustrated that these phenomena can be associated not only to phase errors in the frequency domain of the image but also a 2D modulation effect in the image spectrum. Further research on temporal spectrum of images will be useful to understand and characterize the turbulence-distorted imagery. This study provides a foundation for the development of algorithms to correct turbulence distortion in images. This is achieved by identifying an analytical model for turbulence distortion in acquired imagery. This study also provides a tool to assess the severity of turbulence in imagery. As a result, the user has a tool to determine the usefulness of the measured data.

REFERENCES

[1] Andrews, L. C. and Philips, R. L., [Laser Beam Propagation through Random Media], SPIE Optical Engineering Press, Bellingham, WA (1998).

[2] Roggemann, M. C. and Welsh, B., [Imaging through Turbulence, Boca Ration], CRC Press, FL (1996).

[3] Kolmogorov, A. N., "The local structure of turbulence in incompressible viscous fluids for very large reynolds' number," in [Turbulence, Classics Papers on Statistical Theory], S. K. Friedlander and L. Topper (eds.), pp. 151-155, Wiley-Interscience, New York, NY (1961).

[4] Tatarskii, V. I., [Wave Propagation in a Turbulence Medium], Dover Publications, New York, NY (1967).

[5] Fried, D. L., "Statistics of a geometric representation of wavefront distortion," J. Opt. Soc. Am., Vol. 55, 1427-1435 (1965).

[6] Goodman, J., [Statistical Optics], Wiley & Sons, New York, NY (1985).

[7] Hufnagel, R. E. and Stanley, N. R., "Modulation transfer function associated with image transmission through turbulent media," J. Opt. Soc. Am., Vol. 54, 52-61 (1964).

[8] Fried, D. L., "Optical resolution through a randomly inhomogeneous medium for very long and very short exposures," J. Opt. Soc. Am., Vol. 56, 1372-1379 (1966).

[9] Kopeika, N. S., [A System Engineering Approach to Imaging], Vol. 38 of the SPIE Press Monographs, SPIE Optical Engineering Press, Bellingham, WA (1998).

[10] Watkins, W. R., Crow, S. B., and Kantrowitz, F. T., "Characterizing atmospheric effects on target contrast," Optical Engineering, Vol. 30 (10), 1563-1575 (1991).

[11] Buskila, K., Towito, S., Shmuel, E., Levi, R., Kopeika, N., Krapels, K., Driggers, R. G., Vollmerhausen, R. H., and Halford, C. E., "Atmospheric modulation transfer function in the infrared," Applied Optics, Vol. 43, 471-482 (2004).
[12] Jacobs, E., Vollmerhausen, R., and Tofsted, D., "Psychophysical validation of the NVESD performance model in stmospheric turbulence," Proc. Military Sensing Symposium, Feb (2004).
[13] Millane, R. P., "Recent advances in phase retrieval," Proc. of SPIE Vol. 6316, Image Reconstruction from Incomplete Data IV, 63160E-1 – 11 (2006).
[14] Goldring T. and Carlson, L., "Analysis and implementation of non-kolmogorov phase screens appropriate to structured environments," Proc. SPIE Vol. 1060, Nonlinear Optical Beam Manipulation and High Energy Beam Propagation through the Atmosphere, 244-264 (1989).
[15] Tofsted, D., "Turbulence simulation: on phase and deflector screen generation," U.S. Army Research Laboratory Technical Report, ARL-TR-1886 (2001).
[16] Goodman, J., [Introduction to Fourier Optics], McGraw-Hill, New York, NY (1968).
[17] Soumekh, M., [Fourier Array Imaging], Prentice Hall, Englewood Cliffs, NJ (1994).
[18] Repasi, E. and Weiss, R. "Analysis of image distortions by atmospheric turbulence and computer simulation of turbulence effects," Proc. of SPIE Vol. 6941, Infrared Imaging Systems: Design, Analysis, Modeling, and Testing XIX, 69410S-1-13 (2008).

Acknowledgement

We would like to thank Dr. Joe Mait for his very helpful comments. If you find this manuscript somewhat readable, a large part is due to his willingness to point out things that were not explained clearly and notations that were not well defined. We have followed most of his recommendations. We would also like to thank Dr. Endre Repasi and his group for providing field trial imagery data with turbulence that is utilized in this study.

Appendix A. Signal Propagation Geometry with a Parallel Turbulence

In Fig. 2, x_1 represents the distance from the target to the turbulence, D the width of the turbulence band, and x_3 the distance from the turbulence to the array. Rewrite (7) by using (6) and replacing y_1, y_2, and y_3 with x_1, D, x_3, θ_1, and θ_2, we have

$$x_1 \tan\theta_1 + D n \tan\theta_1 + x_3 \tan\theta_1 - y_t = 0 \text{, where } n = 1/n_2 .$$

Using the single-variable bounded nonlinear function minimization method, the value of $\sin\theta_1$ is solved by minimizing (8), that is,

$$\min_{\theta_1} (x_1 \tan\theta_1 + D n \tan\theta_1 + x_3 \tan\theta_1 - y_t) \text{, where } x_1 = x - D - x_{r0} \text{ and } x_3 = x_{r0}$$

Appendix B. Signal Propagation Geometry with a Slanted Turbulence

In Fig. 3, θ_r represents the slanted angle of the turbulence with respect to the target and sensor plane. The distances of y_1, y_2, and y_3 are calculated as follows:

$$y_1 = (x\cos\theta_r + y\sin\theta_r - x_{r0} - D)\tan\theta_1$$
$$y_2 = D n \tan\theta_1$$
$$y_3 = (x_{r0} + u\sin\theta_r)\tan\theta_1$$

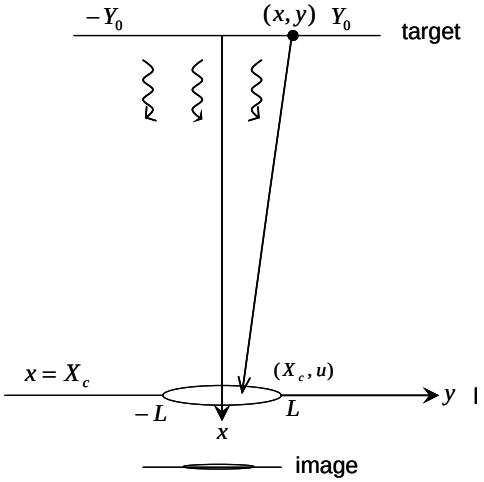

Figure 1. Image formation geometry.

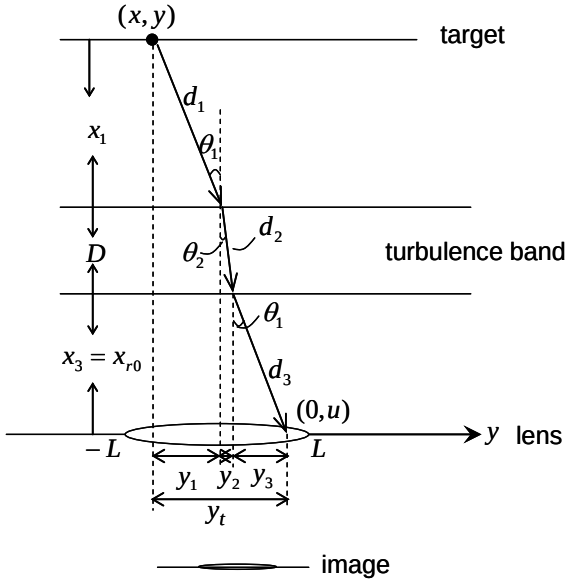

Figure 2. Image formation geometry with parallel turbulence.

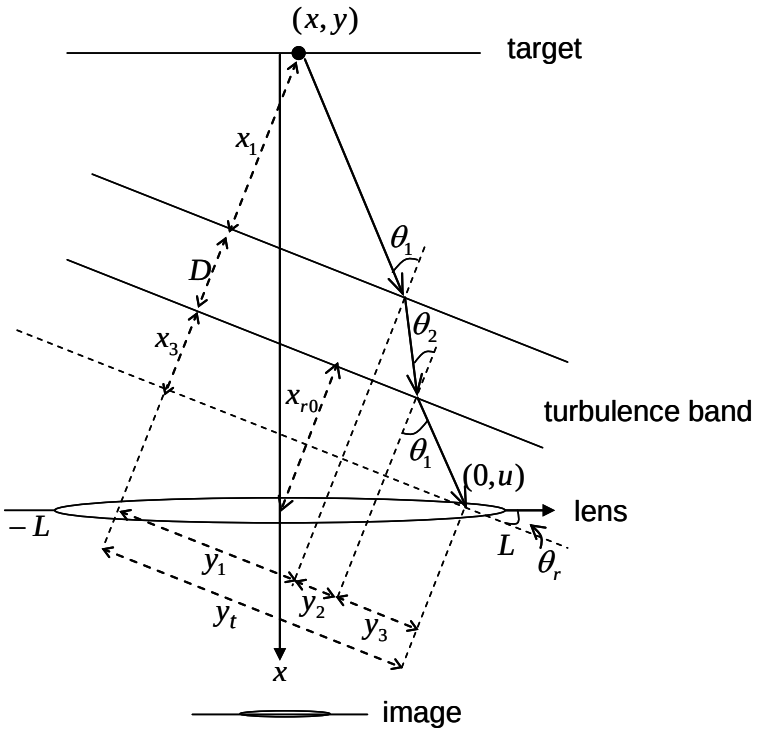

Figure 3. Image formation geometry with slanted turbulence.

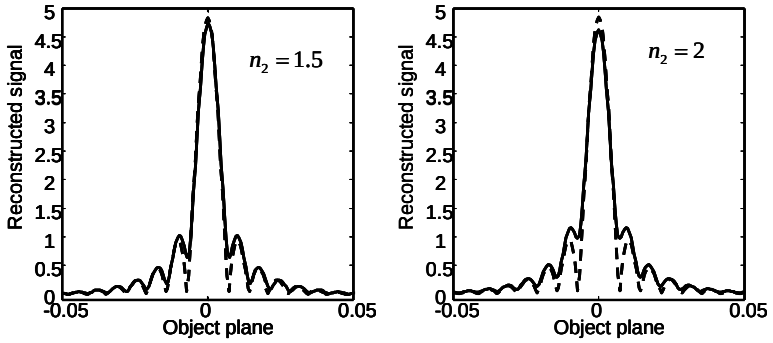

Figure 4. Varying the turbulence index of refraction. The solid lines represent the magnitude of signal with turbulence, $g(y)$, the dotted lines the signal without turbulence, $g_1(y)$. This indicates that larger index of refraction of the turbulence causes more degradation of the signal.

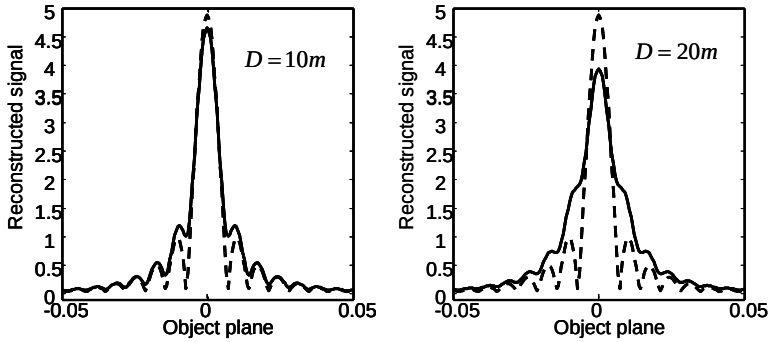

Figure 5. Varying the turbulence width. The solid lines represent the magnitude of signal with turbulence, $g(y)$, the dotted lines the signal without turbulence, $g_1(y)$. This also indicates that the thicker layer of the turbulence causes more degradation of the signal.

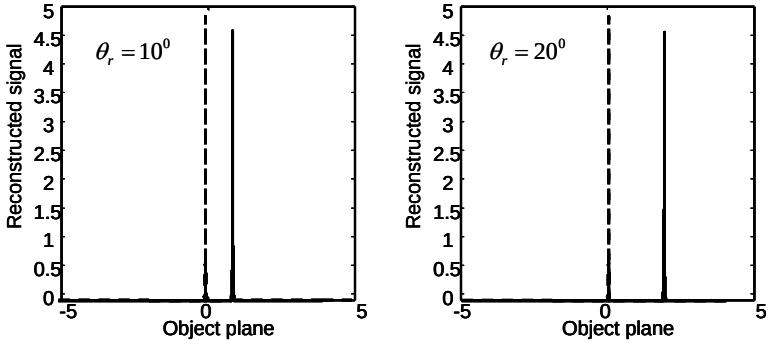

Figure 6. Varying the turbulence slanted angle. The solid lines represent the magnitude of signal with turbulence, $g(y)$, the dotted lines the signal without turbulence, $g_1(y)$. A turbulence slanted angle causes a shift between two signals. When the slanted angle of the turbulence increases, this shift increases too.

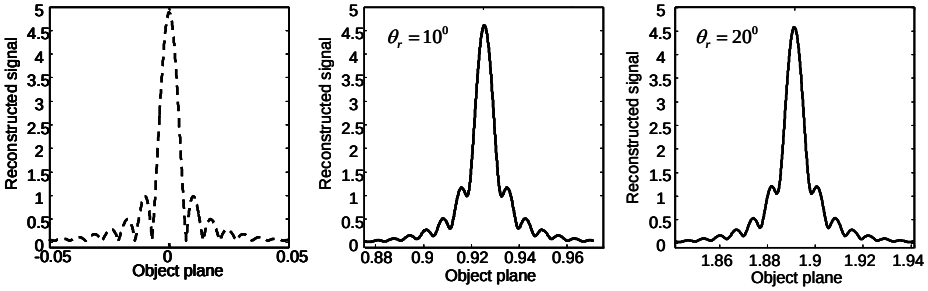

Figure 7. Varying the turbulence slanted angle (con't). Zoomed in version of Figure 6. The solid lines represent the magnitude of signal with turbulence, $g(y)$, the dotted lines the signal without turbulence, $g_1(y)$.

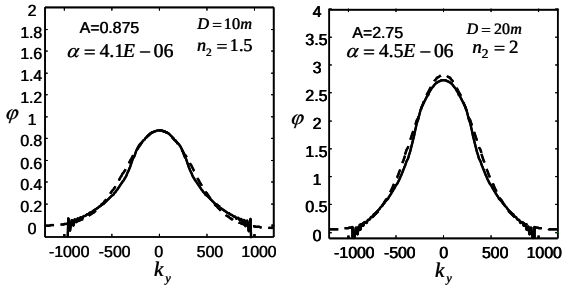

Figure 8. Phase angle of the correlation function for varying D and n_2. The solid lines represent the phase angle of the correlation, dotted lines the fitted Gaussian function curves, and the parameters (A, α) used to fit the Gaussian functions.

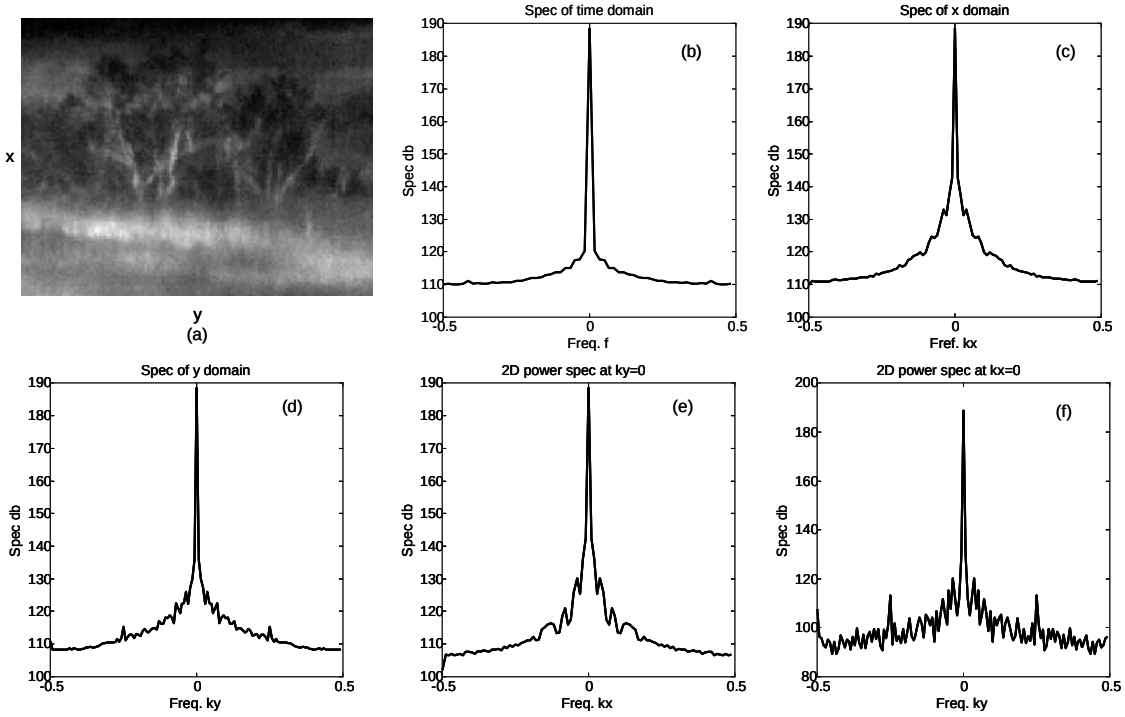

Figure 9. Spectral and 2D power spectral properties of a natural scene.

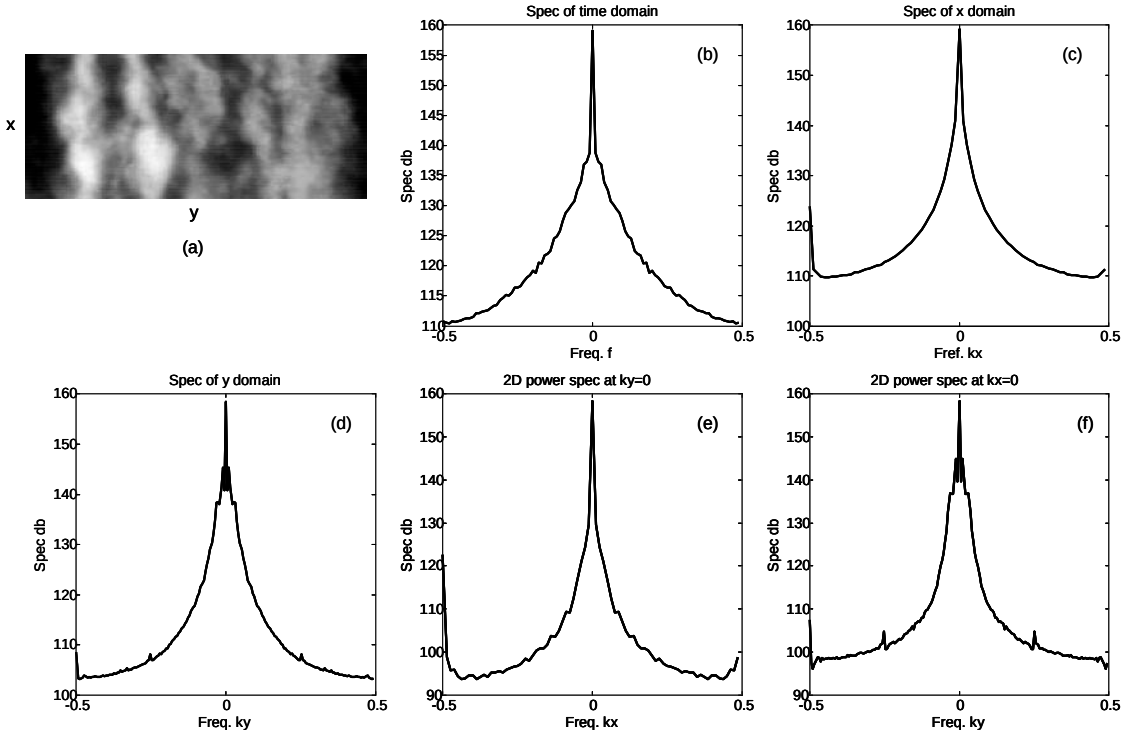

Figure 10. Spectral and 2D power spectral properties of a test pattern scene with strong turbulence.

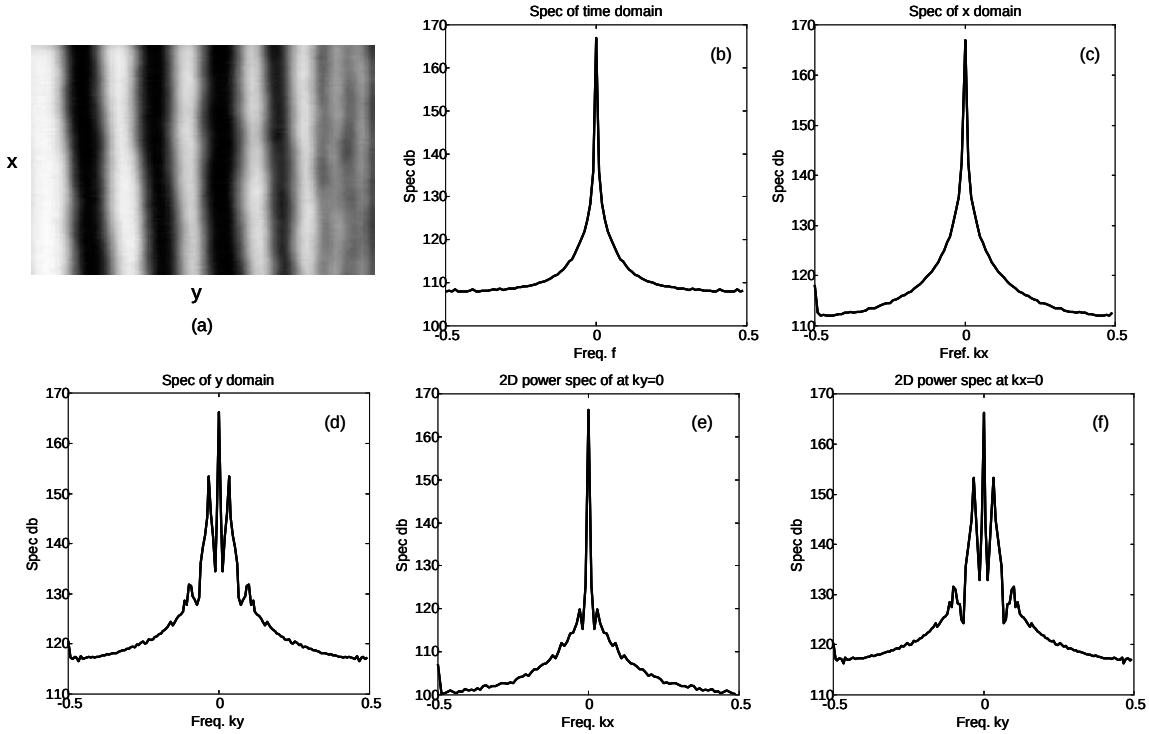

Figure 11. Spectral and 2D power spectral properties of a test pattern scene with weak turbulence.

ADMNSTR
DEFNS TECHL INFO CTR
ATTN DTIC OCP V MADDOX
8725 JOHN J KINGMAN RD STE 0944
FT BELVOIR VA 22060-6218

US ARMY NIGHT VISION & ELECTRONICS SENSORS DIRECTORATE
SENSOR PERFORMANCE BRANCH
ATTN AMSRD-CER-NV-MS-SP J REYNOLDS
ATTN AMSRD-CER-NV-MS-SP R ESPINOLA
ATTN J CHA
ATTN K KRAPELS
10221 BURBECK RD
FT BELVOIR VA 22060

NAVAL RESEARCH LABORATORY
ATTN R G DRIGGERS
4555 OVERLOOK AVE
WASHINGTON DC 20375

US ARMY RSRCH LAB
ATTN RDRL CIM G T LANDFRIED
BLDG 4600
ABERDEEN PROVING GROUND MD 21005-5066

US ARMY RSRCH LAB
ATTN IMNE ALC HRR MAIL & RECORDS MGMT
ATTN RDRL CIM L TECHL LIB
ATTN RDRL CIM P TECHL PUB
ATTN RDRL SE J PELLEGRINO
ATTN RDRL SES E R RAO
ATTN RDRL SES E S S YOUNG (10 COPIES)
ATTN RDRL SES J EICKE
ADELPHI MD 20783-1197